

# Identifying Lightning Processes in ERA5 Soundings with Deep Learning

Gregor Ehrensperger<sup>1, 2</sup>, Thorsten Simon<sup>2</sup>, Georg J. Mayr<sup>2</sup>, and Tobias Hell<sup>1</sup>

<sup>1</sup>Data Lab Hell GmbH, Austria

<sup>2</sup>Department of Atmospheric and Cryospheric Sciences, University of Innsbruck

**Correspondence:** Gregor Ehrensperger (gregor.ehrensperger@uibk.ac.at)

**Abstract.** Atmospheric environments favorable for lightning and convection are commonly represented by proxies or parameterizations based on expert knowledge such as CAPE, wind shears, charge separation, or combinations thereof. Recent developments in the field of machine learning, high resolution reanalyses, and accurate lightning observations open possibilities for identifying tailored proxies without prior expert knowledge.

To identify vertical profiles favorable for lightning, a deep neural network links ERA5 vertical profiles of cloud physics, mass field variables and wind to lightning location data from the *Austrian Lightning Detection & Information System (ALDIS)*, which has been transformed to a binary target variable labeling the ERA5 cells as *cells with lightning activity* and *cells without lightning activity*. The ERA5 parameters are taken on model levels beyond the tropopause forming an input layer of approx. 670 features. The data of 2010–2018 serve as training/validation.

On independent test data, 2019, the deep network outperforms a reference with features based on meteorological expertise. SHAP values highlight the atmospheric processes learned by the network which identifies cloud ice and snow content in the upper and mid-troposphere as very relevant features. As these patterns correspond to the separation of charge in thunderstorm cloud, the deep learning model can serve as physically meaningful description of lightning.

Depending on the region, the neural network also exploits the vertical wind or mass profiles to correctly classify cells with lightning activity.

## 1 Introduction

Lightning affects many fields of our everyday’s life. Cloud-to-ground flashes might hit infrastructure such as wind turbines (Becerra et al., 2018) and power lines (Cummins et al., 1998) and thus cause power outages. Humans might get injured (Ritenour et al., 2008) or even die (Holle, 2016) after being hit by lightning. Wildfires (Reineking et al., 2010) release carbon dioxide into the climate system, and thus limit the biosphere’s capacity to store carbon dioxide. Lightning also affects the climate system by producing nitrogen oxides which play a key role in ozone conversion and acid rain production (DeCaria et al., 2005). Ozone is an important greenhouse gas and changes in concentration can lead to warming or cooling of the atmosphere. Thus, understanding of lightning is also an important factor in climate change research (Finney et al., 2018).

Given lightning's impact and that an average of 46 flashes are occurring around the globe every second (Cecil et al., 2014) it is desirable to have models of the atmosphere capable to simulate lightning and its underlying dynamic processes down to the resolved scales of the numeric model. Beyond the resolved scales one relies on so called proxies *or* parameterization to further describe lightning. The term *proxy* is commonly used for quantities derived from atmospheric model output *after* numeric computations. *Parameterizations* mean the description of lightning *while* numeric computations of the atmosphere model.

Proxies are frequently applied to assess historic and future behavior of convection and lightning. Popular proxies are cloud top height (Price and Rind, 1992), cloud ice flux (Finney et al., 2014), CAPE times precipitation (Romps et al., 2018), or the lightning potential index (Brisson et al., 2021). Though, these proxies perform reasonably good (Tippett et al., 2019), there is a need for more complex or holistic proxies, as the behavior of lightning in a changing climate is still uncertain (Murray, 2018). Another application that makes clear that more research on the description of lightning is needed in the field of operational weather forecasting. Experience shows, for instance, that CAPE needs to be adapted to local conditions in order to perform well (Groenemeijer et al., 2019).

Parameterizations are an internal part of numeric models, as they emulate sub-scale processes that cannot be resolved due the discretization of governing equations. Therefore, the emulated processes give feedback to the other processes, also on larger scales, within the atmospheric model. For instance, Tost et al. (2007) showed that modeled nitrogen oxide is sensitive to lightning parameterizations in numerical models. Next to the classic description of lightning using cloud top height (Price and Rind, 1992), parameterizations have been developed using polynomial regression (Allen and Pickering, 2002) and schemes based on hydrometeors in the mixed-phase region which is important for cloud-resolving models (McCaul et al., 2009). A comparison of several parameterizations using a superparameterized model is given by Charn and Parishani (2021). Recently, the ECMWF launched a product for total lightning densities expressed as a function of hydrometeors contents, CAPE, and (convective) cloud-base height output by the convective parameterization (Lopez, 2016).

In recent years machine learning (ML) approaches have been proposed to describe convection and lightning. Forty pre-selected single level parameters from ERA5 were processed by artificial neural networks and gradient boosting machines for lightning in parts of Europe and Sri Lanka (Ukkonen et al., 2017; Ukkonen and Mäkelä, 2019). The authors also bring up the idea to feed ERA5's model level parameters directly to an appropriate ML tool, i.e. neural network. Other studies tested random forests for regions such as the Hubei Province in China (Shi et al., 2022) or the Southern Great Plains (Shan et al., 2023) and generalized additive models (GAM) for the European Alps (Simon et al., 2023). All these studies confirm that the use of ML approaches for the description of lightning is promising. In concurrent research, also *explainable artificial intelligence* (XAI) techniques are used to move towards understanding the underlying reasoning of complex AI models and shows encouraging results in Earth System Sciences applications (Barnes et al., 2020; Dutta and Pal, 2022; Hilburn et al., 2021; Mayer and Barnes, 2021; Stirnberg et al., 2021; Toms et al., 2021). Silva et al. (2022) use XGBoost classification trees to explore when the NASA Goddard Earth Observing System model of lightning flash occurrence shows weaknesses and apply *Shapley additive explanations* (SHAP) to describe which meteorological drivers are related to the model errors. They found that these errors are strongly related to convection in the atmosphere and certain characteristics of the land surface.

This paper builds upon these studies and aims at finding a *holistic* description of lightning. Supervised deep learning harvests temporally and vertically well resolved ERA5 soundings of atmospheric dynamics and cloud physics to explain observations from the *Austrian Lightning Information & Detection System* (ALDIS). The pattern found in ERA5 serve as proxy, but could also guide towards a parameterization of lightning. Using ERA5 on model levels comes with the benefit that a complete picture of the atmosphere is considered to find patterns explaining lightning. As the approach sees the *raw model atmosphere*, no expert parameters diagnosed from the model levels are used as inputs, the study also answers whether deep learning can identify physically meaningful patterns within the ERA5 sounding to describe lightning processes.

The region of interest are the eastern Alps which are characterized by complex terrain. Atmospheric dynamics on a gamut of scales interacting with topography, which lead to various meso-scale (Feldmann et al., 2021) and local processes (Houze, 2012) that can trigger convection and lightning. This study focuses on lightning during the peak phase of the warm season (June, July, August) which differs fundamentally in the underlying dynamic processes to lightning during the cold season (Morgenstern et al., 2022). Morgenstern et al. (2023) show that there are different environments, either dominated by wind-field or mass-field variables, that favor lightning depending on the region.

The paper is structured as follows. Section 2 presents both the lightning detection data and the atmospheric reanalyses, which both enter the supervised deep learning approach and a reference model (Sect. 3). Additionally, Section 3 illustrates the methods to analyze performance and explainability of the deep learning approach. The results of these analyses are given in Section 4. Section 5 discusses the physical patterns identified by the method, scrutinizes further applications and research that is made possible with the novel insights and finally concludes the study.

## 2 Data

Two data sets build the foundation for this supervised machine learning task. First, the observational data from the lightning location system ALDIS (Sect. 2.1) is used to derive the labels distinguishing cells with and without lightning activity. Second, pseudo soundings from ERA5 (Sect. 2.2) serve as input for the deep learning approach. Spatially, the grid centers range from  $8.25^{\circ}E$  to  $16.75^{\circ}E$  and from  $45.25^{\circ}N$  to  $49.75^{\circ}N$ . Temporally, data for the meteorological summers (June, July, August) from 2010 to 2019 are available.

### 2.1 Lightning Detection Data

The Austrian Lightning Detection & Information System (ALDIS) is part of the European effort EUCLID (Schulz et al., 2016). Cloud-to-ground flashes with a current of  $> 15$  kA or  $< -2$  kA are aggregated to the spatio-temporal grid cells of ERA5 (Sect. 2.2). Each cell has a horizontal extent of approx.  $30 \text{ km} \times 30 \text{ km}$  and temporally of one hour. If at least one flash has been detected in such a grid cell, then the cell is labeled as *cell with lightning activity*. Otherwise, if not a single flash has been detected, the cell is labeled as *cell without lightning activity*.

**Table 1.** ERA5 parameters on model levels.

Name	Short Name	Units	Parameter ID
Temperature	t	$K$	130
Specific humidity	q	$kg\,kg^{-1}$	133
U component of wind	u	$m\,s^{-1}$	131
V component of wind	v	$m\,s^{-1}$	132
Vertical velocity	w	$Pa\,s^{-1}$	135
Specific rain water content	crwc	$kg\,kg^{-1}$	75
Specific snow water content	cswc	$kg\,kg^{-1}$	76
Specific cloud liquid water content	clwc	$kg\,kg^{-1}$	246
Specific cloud ice water content	ciwc	$kg\,kg^{-1}$	247

## 2.2 Atmospheric Reanalysis

ECMWF’s fifth reanalyses, ERA5 (Hersbach et al., 2020), is available at a horizontal resolution of  $0.25^\circ$  and temporally of 1 hour. Vertically it consists of 137 hybrid model levels that align with topography near ground and approach isobars in the upper atmosphere (see <https://confluence.ecmwf.int/display/UDOC/L137+model+level+definitions>). On these model levels nine parameters (Tab. 1) are available to describe the state of the atmosphere. Next to classical parameters, temperature, specific humidity and three-dimensional winds, ERA5 provides a description of liquid and solid water particles in clouds, i.e. the specific content of ice, snow (including graupel), liquid water, and rain. For this study, these parameters are used on the lowest 74 model levels, spanning from level number 64 (approx. 15 000 m geopotential height) to level number 137 (10 m above ground).

## 2.3 Composition of Datasets

The two data sets are merged in order to obtain a tabular data shape. Each row of this tabular data refers to a spatio-temporal grid cell. Thus, it can be indexed by the longitude and latitude of its center as well as its hourly time stamp. Each row is either labeled as cell with lightning activity or without lightning activity. The nine ERA5 parameters (Tab. 1) on their 74 model levels enter the tabular data such that each resulting column refers to an *individual* parameter on an *individual* level, making up a total of  $9 \times 74 = 666$  ERA5 feature columns. Further, each row is complemented with the information of the *hour of the day* and *day of the season* to account for diurnal and seasonal variations, respectively. Finally, the model topography is added as another column.

### 3 Methods

To avoid incorporating expert knowledge by using specialized deep learning architectures, a classical fully connected deep neural network (Sect. 3.1) is used to fit a model which capable of distinguishing whether a specific spatio-temporal grid cell corresponds to a lightning cell. To make sure that the neural network can model lightning sufficiently well, the resulting outputs are compared to those of a state-of-the-art reference model (Sect. 3.2) on unseen test data. Finally, insights into the patterns exploited by the trained model are gained by applying Shapley additive explanations (Sect. 3.3).

#### 3.1 Deep Learning Approach

A rather general fully connected neural network was designed, consisting of eight hidden layers with  $512 \times 512 \times 512 \times 512 \times 128 \times 128 \times 128 \times 16$  nodes. Leaky rectified linear unit (leaky ReLU) is used as activation function for all hidden layers. The input dimension is predetermined by the number of input features and thus equals 671 (nine atmospheric variables on 74 levels, longitude, latitude, hour of the day, day of the season, and topography). The dimension of the output layer equals one, as it solely classifies whether the cell is with or without lightning activity. The model output is activated with the sigmoid function. The input features are scaled, such that the nine atmospheric variables are standardized by considering the 74 levels altogether, prior training. To prevent the model from overfitting, dropout (Srivastava et al., 2014) with a value of 0.15 and early stopping with a patience of ten epochs are applied. Binary cross entropy serves as loss function with a weight of approximately 41 for positive events (flash occurrences) to address for the highly imbalanced data set.

#### 3.2 Reference Model

For reference a generalized additive model (GAM, Wood, 2017) is used. This model is trained on longitude, latitude, hour of the day, day of the season, topography and the atmospheric variables listed in Tab. 2, which were derived from ERA5 soundings on meteorological expertise (Simon et al., 2023).

Thus, the input dimension for the reference model is only 15. The GAM is fitted using an algorithm tailored for gigadata (Wood et al., 2017).

#### 3.3 Explainability

While generalized additive models are interpretable by users (Lou et al., 2012), interpretability research of deep neural networks still suffers many gaps (Zhang et al., 2021). Deep SHAP (Lundberg and Lee, 2017) is utilized to gain insights into the patterns exploited by the neural network from Section 5 and to understand the features contributing to the classification of a spatio-temporal cell as one exhibiting lightning activity. SHAP is a game theoretic approach to explain the relation of input and output of any machine learning model. It uses the concept of Shapley values (Shapley, 1952) to provide local interpretability by computing feature attributions which lead to the model’s output for a given input. Unfortunately, the computation time for calculating the exact Shapley values grows exponentially with the number of input features. Common implementations for computing Shapley values use simplifications to ensure computational feasibility.

**Table 2.** The reference model is trained using the following ten atmospheric variables.

Description	Short Name
Convective available potential energy	cape
Binary indicator whether cloud is present	cloud_exists
Convective precipitation	cp
Mass of specific snow water content between the $-20^{\circ}C$ and $-40^{\circ}C$ isotherms	cswc2040
Cloud top height in height above ground	cth
Instantaneous surface sensible heat flux	ishf
Medium cloud cover	mcc
Total column supercooled liquid	tcslw
Mass of water vapor between the $-10^{\circ}C$ and $-20^{\circ}C$ isotherms	wvc1020
Two meter temperature	2t

This work applies Deep SHAP which is a model agnostic method that leverages extra knowledge about the nature of deep neural networks to approximate Shapley values more efficiently but also assumes independence among the input features. As in various applications, this property obviously is not fulfilled in the given data set but using a more accurate approximation as described in Aas et al. (2021) is not feasible with the large number of input features. Despite this formal prerequisite, SHAP values are successfully utilized in a variety of imaging tasks (e.g. in the medical field (van der Velden et al., 2022)) although the independence assumption is also heavily violated when images are used as input and every pixel serves as an individual input feature. Understanding the raw ERA5 vertical profiles as a collection of 1D-images it is safe to assume that Deep SHAP leads to sufficiently good approximations to the precise Shapley values and can therefore be applied to gain insights into the neural network trained in this study.

## 4 Results

This section first investigates the performance of the deep learning approach by comparing its output on unseen test data against observations and the output of the reference model (Sect. 4.1). Next, the application of SHAP allows to gain insights about the vertical profiles exploited by the neural network which indicate the occurrence of lightning (Sect. 4.2).

### 4.1 Performance of the deep learning approach

The neural network is trained as described in Sect. 3.1 to distinguish whether a given spatio-temporal cell is a cell with or without lightning activity. To map the output of the model to a binary category, a threshold has to be defined. The threshold is determined by maximizing the  $F_1$  score, which symmetrically represents precision and recall in one metric, on the validation set.

The reference model is fitted as described in Sect. 3.2 and the threshold is computed following the same procedure.

**Table 3.** Confusion matrices of the neural network model (left) and the reference model (right) on test year 2019.

		observed		observed	
		yes	no	yes	no
modeled	yes	14 370	61 446	12 654	65 176
	no	15 768	1 374 741	17 484	1 371 011

The resulting confusion matrices are displayed in Tab. 3. The neural network slightly outperforms the reference model in every category of the confusion matrix on previously unseen test data (year 2019). This can also be seen by comparing the *Matthew correlation coefficients* (mcc) of the two models, where +1 represents a perfect match between model output and observations, and 0 no better than random guessing. The deep learning model has an mcc of approximately 0.278 and the reference model 0.237.

Previous studies have shown that descriptions of lightning based on ML models reproduce the observed diurnal cycle more realistically than simple proxies such as CAPE (Fig 2. in Simon et al., 2023). To investigate the ability of the introduced model to reproduce the diurnal cycle of lightning, the mean of the binary model output and the observations of the test year 2019 for each hour of the day is calculated for four different small subdomains (Fig.1). In this case, the model’s threshold is calibrated to align the average predicted and observed lightning frequencies of the validation set.

The comparison reveals a good match of the shapes of the modeled and observed diurnal cycles. In particular, the transition from the low values in the morning to the peak in the afternoons are well reproduced. For three of the subdomains (Flatlands, Northern Alpine Rim and Southern Alpine Rim), the model slightly overestimates the observed occurrence probabilities, which is a result of different mean occurrences of lightning in the validation (used for finding the threshold) and test data (plotted). The only larger deviation can be found during the late afternoon in the High Alps, where the model overestimates the observed diurnal cycle. It should be noted that the curves of the reference model are not directly comparable to those presented in (Fig. 2 in Simon et al., 2023), despite using the same model architecture and input variables. This discrepancy arises from the fundamentally different data strategies employed. Simon et al. (2023) implemented a cross-validation method across the entire dataset spanning 2010 to 2019, averaged the calibrated probabilities for lightning occurrences and evaluated the mean of the modeled diurnal cycles over the ten years of available data. In contrast, the current study exclusively utilizes data from the years 2010 to 2018 to fit the model and threshold. The model’s performance and resulting diurnal cycles are then assessed using data exclusively from the full year 2019, which has previously not been seen.

#### 4.2 Identifying patterns exploited by the deep learning model

The good performance of the deep learning approach motivates a closer look at what patterns the model has learned in order to distinguish between cells with and without lightning activity. SHAP values (Sect. 3.3) indicate which inputs the neural network is particularly interested in. Since the goal is to find patterns which are valid throughout the full region used for training, and

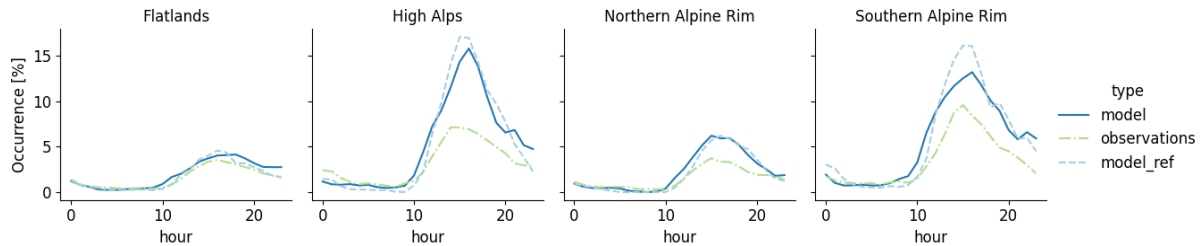


**Figure 1.** Diurnal cycles of the probability of a lightning occurring in a spatio-temporal cell. The binary model outputs of the neural network and reference model, as well as the binary observations have been averaged over four subdomains.

unbiased by the frequency of lightning within a specific spatial cell, the SHAP values are computed separately for each spatial cell.<sup>1</sup> Given a specific input, the SHAP values of all input features always sum up, with only small approximation errors, to the difference between the base value (derived from the expected model output based on background data) and the model output. To better understand the underlying patterns, the SHAP values are scaled by dividing them by the difference between the base value of the corresponding spatial cell and the threshold at which a cell is classified as having lightning activity. This implies that the model classifies a cell as having lightning activity as soon as the scaled SHAP values sum up to one or more, regardless of the underlying base value. All plots in this paper illustrate these scaled SHAP values. The aggregated results of the scaled SHAP values of correctly classified cells with lightning activity are visualized in Fig. 2.

On average cloud ice (ciwc) and snow water content (cswc) contribute the most to the network’s output. Also note that ciwc with its lighter-weighted ice crystals is particularly interesting at a geopotential height of approx. 8000 to 12000 m and cswc with its solid precipitation at approx. 3000 to 10000 m.

Taking a closer look (Fig. 3) at the ciwc and cswc at these altitudes, it is noticeable that the model exhibits greater confidence when ciwc and cswc values are substantially elevated. Furthermore, there is a tendency for the model to produce false positives during periods of high ciwc and cswc, while false negatives are more prevalent when these values are low compared to correctly classified lightning events.

While classifications where a cloudy atmosphere is the most dominantly exploited feature by the neural networks are the majority, grouping the results into three categories, following Morgenstern et al. (2023), reveals additional patterns:

`cloud`: True positives where the sum of scaled SHAP values of ciwc, clwc, crwc and cswc exceeds 0.5.

`mass`: True positives where the sum of scaled SHAP values of q and t exceeds 0.5.

`wind`: True positives where the sum of scaled SHAP values of u, v and w exceeds 0.5.

Visualizing the vertical profiles of the scaled SHAP values (Fig. 4a) and the real feature values (Fig. 4b) of these three groups it becomes clear that the mass-field lightning is characterized by warmer temperatures in the troposphere, a less stable stratifi-

<sup>1</sup>In particular, within SHAP’s DeepExplainer the full number of samples without lightning activity of the corresponding spatial cell are used as background data.



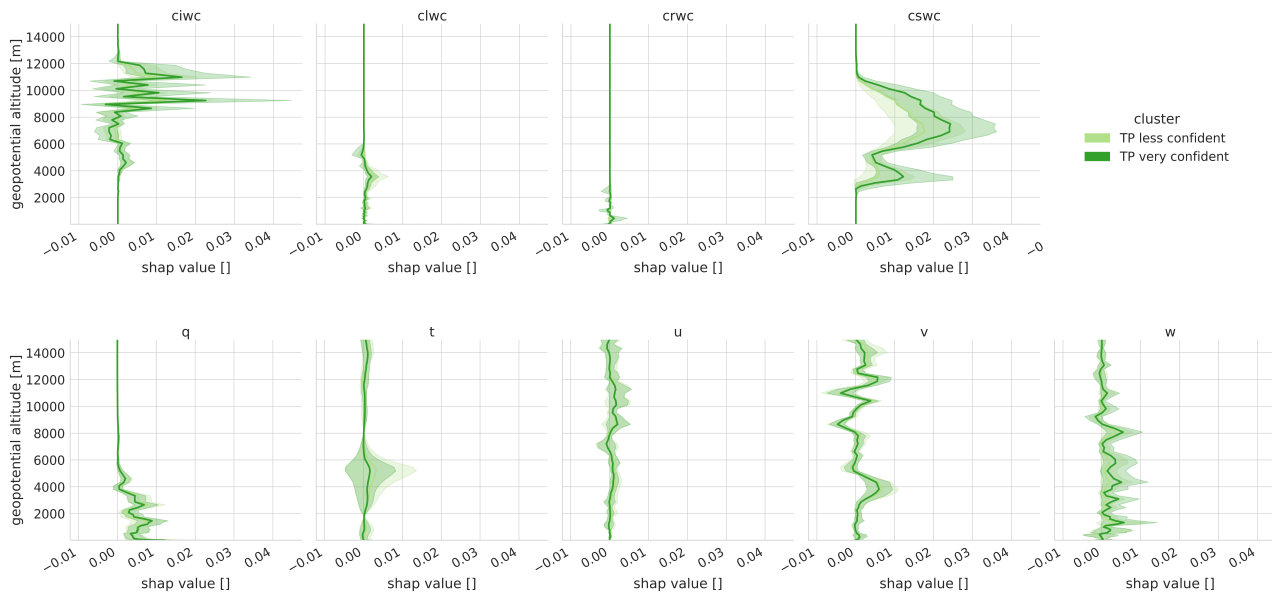


**Figure 2.** Scaled SHAP values for several variables (names on top of each subfigure) on correctly modeled lightning events (true positives). The two colors represent the confidence (stratified by median) of the network in its output. The dark green color summarizes the events where the network is very confident that a lightning event occurred. The light green color summarizes the events where the network still modeled correctly, but with less confidence. The solid lines show the median of all observations and the colored areas highlight the 50% quantiles.

cation and copious amounts of water vapor in the lower troposphere. Larger amounts of latent heat released by condensation as indicated by large *clwc* values in the lower troposphere combined with a weaker stratification result in more CAPE that can be released, which carries solid particles (*ciwc*) higher into the troposphere. Heavier solid hydrometeors (*cswc*) peak further below.

Ice crystals and solid hydrometeors in wind-field lightning, on the other hand, are not transported that far up into the troposphere and they both peak in a similar altitude range. The large-scale vertical velocity in the lower troposphere is high as is the horizontal wind speed – particularly its southern component. Temperatures and consequently specific humidity *q* are lower and the stratification is stabler than for the mass-field lightning. All of this indicates forced lifting along (cold) fronts and topography. Cold fronts in this region typically occur in southwesterly flow downstream of the trough axis, which explains the exceptional values of the *v*-component of the wind. Charge separation consequently occurs on a tilted instead of a nearly vertical path as in mass field lightning, having earned this type of lightning the name *tilted thunderstorm* (Brook et al., 1982; Takeuti et al., 1978; Takahashi et al., 2019; Wang et al., 2021).

Following the approach of Morgenstern et al. (2023), Fig. 5 subdivides the cloud-dominant group into two subcategories: cloud-mass and cloud-wind. This grouping is based on whether the aggregate of scaled SHAP values is greater for mass-related or wind-related parameters.

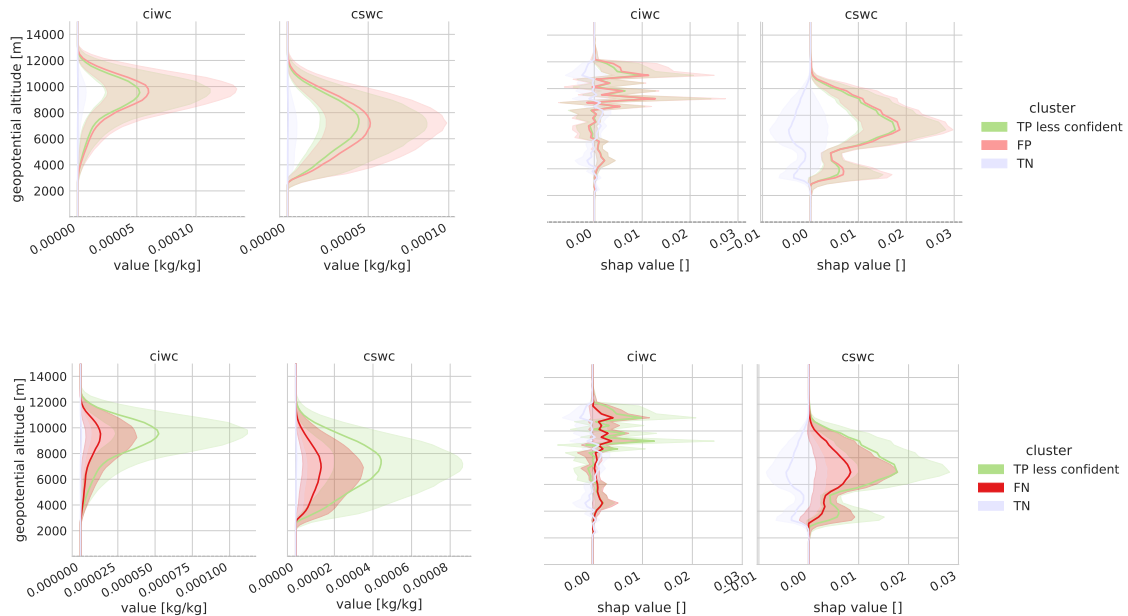


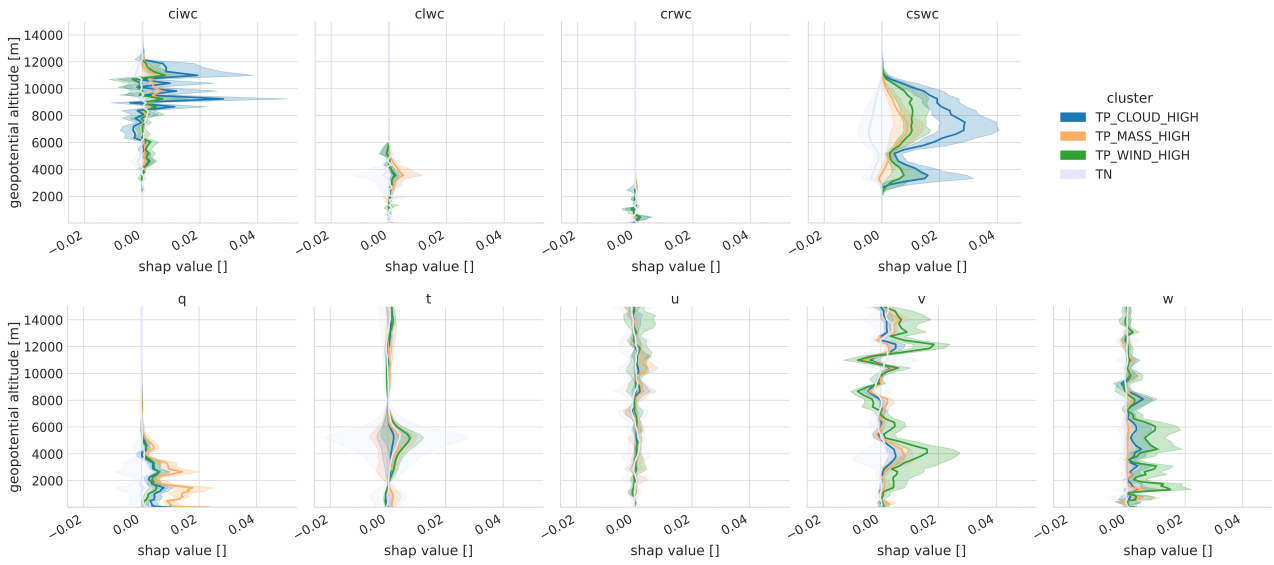
**Figure 3.** The two left columns display the vertical profiles of the real feature labels, while the two right columns present the vertical profiles of the scaled SHAP values. The upper row illustrates less confident true positives (TP) compared to false positives (FP), while the lower row illustrates less confident true positives compared to false negatives (FN). True negatives (TN) are also included for reference.

Lightning with large scaled SHAP and real values of the cloud variables seems to occur for both mass-field and wind-field lightning confirming the results from Morgenstern et al. (2022, 2023), who had used principal component analysis and clustering for identifying these categories.

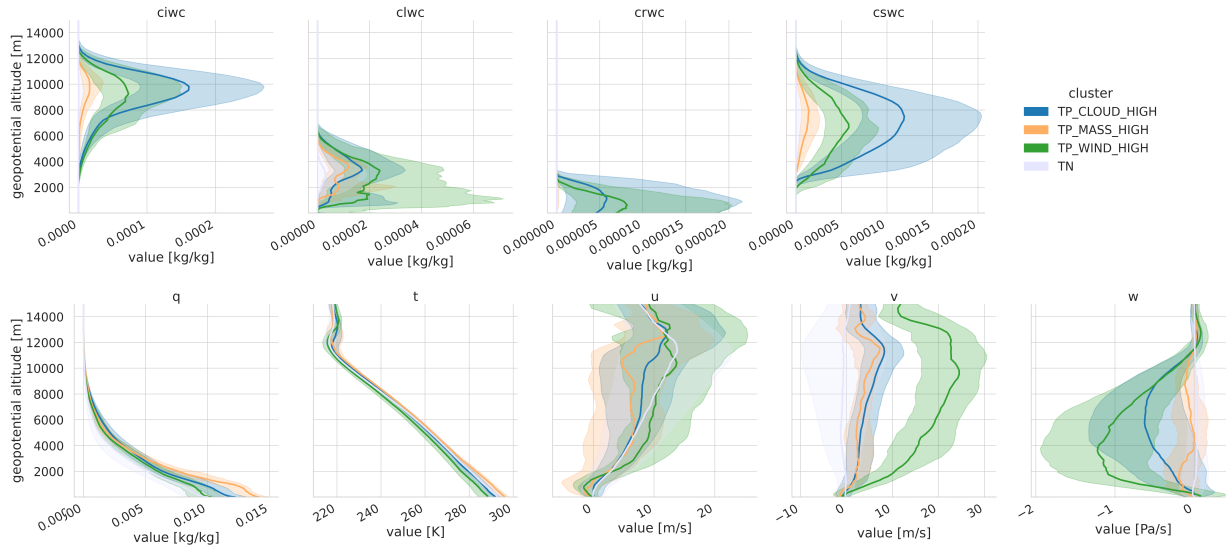
Fig. 6 highlights the geographical regions, where cloud-mass-, cloud-wind-, mass-, or wind-dominant cells exhibiting lightning activity were classified. Cloud-dominant cells with lightning activity are distributed across the entire map, but are particularly abundant along the primary chain of the Alps. Mass-dominant cells are predominantly situated in Northern Italy and Slovenia. Wind-dominant cells are primarily concentrated in the northwestern region of the Italian flat terrain, the Po Plain.

### 4.3 Sample case study

A sample case on unseen test data illustrates how the model from the deep learning approach *sees* a specific weather event. In the afternoon of June 20, 2019, a weak upper level trough embedded in southwesterly flow passed over the Alps, whereas below crest height the flow was predominantly around the Alps. Lightning in the target area (Fig. 7) occurred in the warm sector in a zone with the highest values of equivalent potential temperature. Its accompanying front had just arrived on the west coast of Europe. The lightning model correctly identified lightning in the eastern half of Fig. 7 while misclassifying several occurrences in its western half.

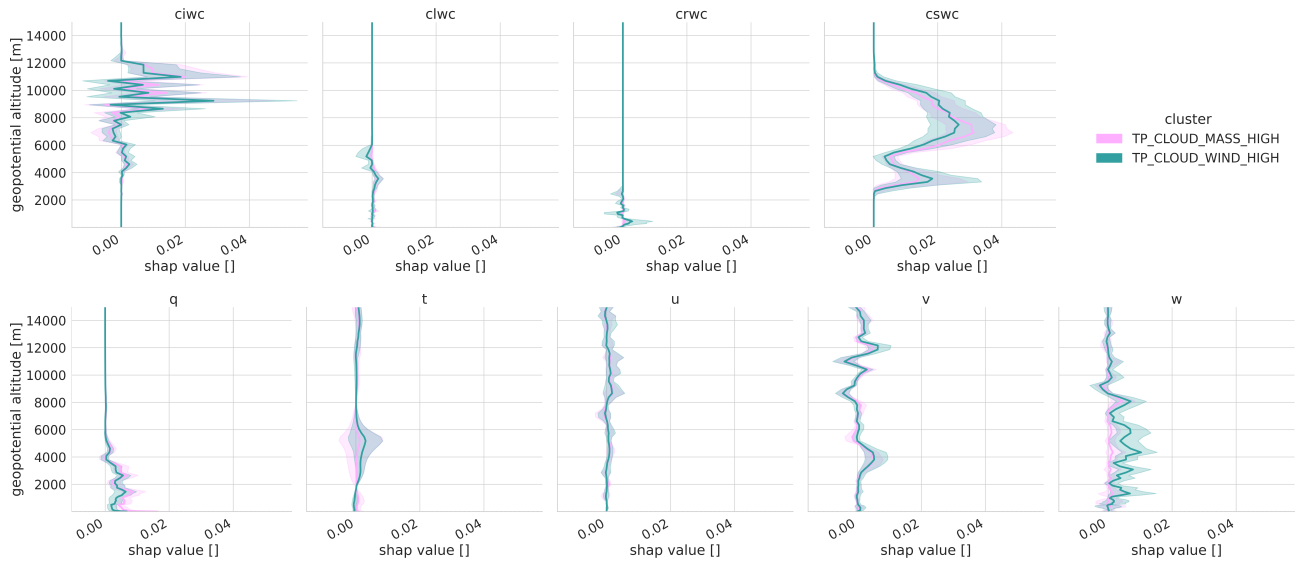


(a) scaled SHAP values

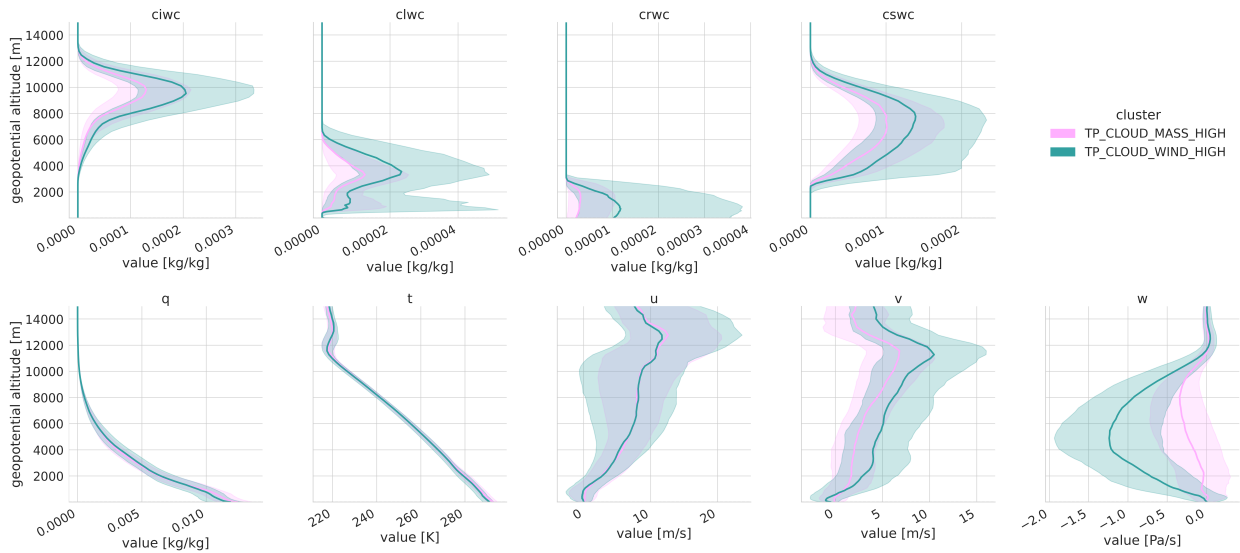


(b) real features

**Figure 4.** Vertical profiles of the scaled SHAP-values (a) and real features (b) per variable with colors indicating true negatives and different groups of true positives (cloud-, mass-, wind-dominant).



(a) scaled SHAP values



(b) real features

**Figure 5.** Vertical profiles of the scaled SHAP-values (a) and real features (b) per variable with colors indicating cloud-mass and cloud-wind dominant true positives.

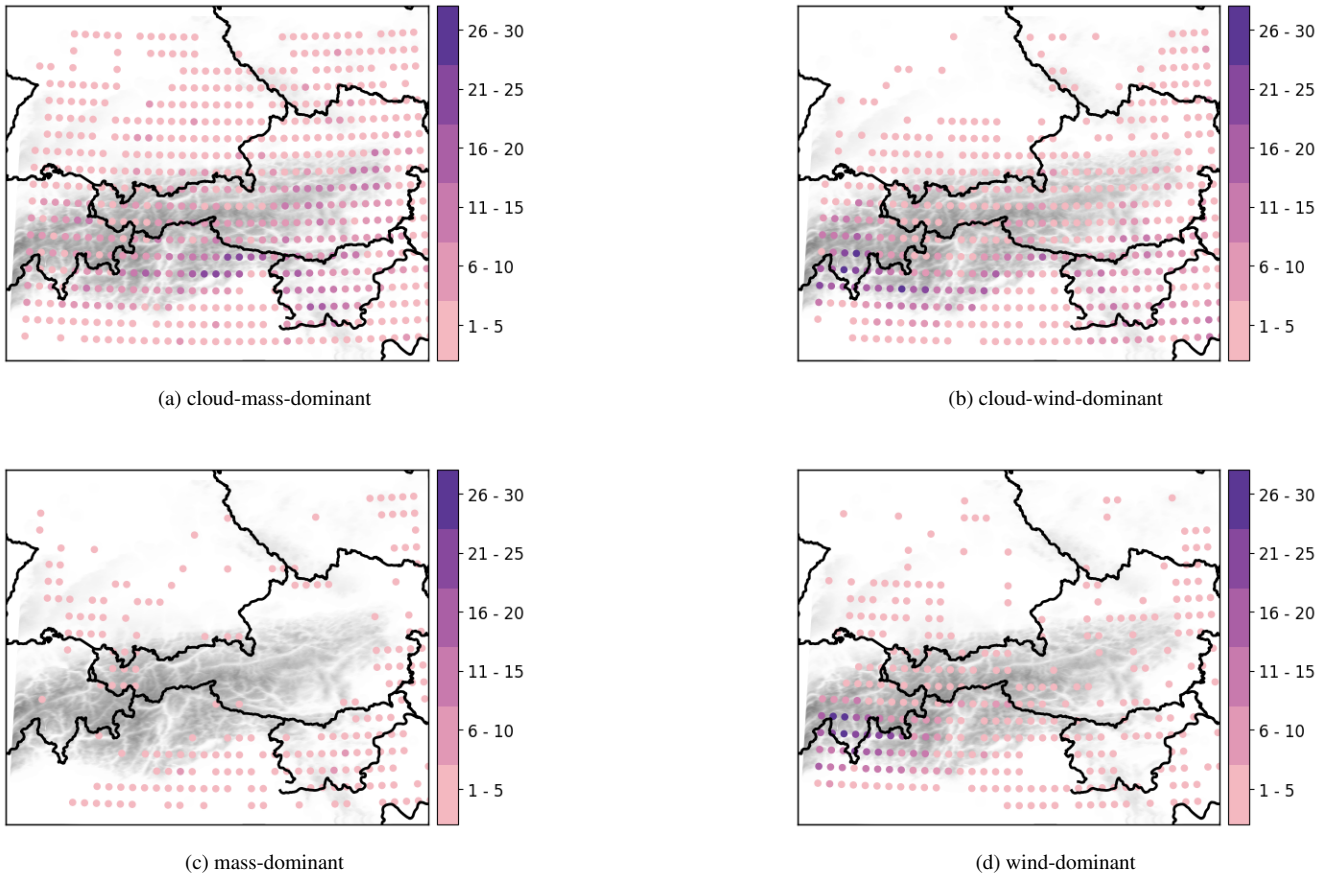


**Figure 6.** The count of true positive classifications stratified by the variable group that is most dominant for each geographical location. The data for the displayed topography layer is taken from TanDEM-X (Rizzoli et al., 2017).

## 5 Discussion and Conclusions

In this study a neural network is trained on the vertical columns of raw ERA5 data without inducing any further expert knowledge about atmospheric processes to classify whether there was a lightning event or not. Then SHAP values are used to explain which variables and vertical levels attribute the most to correct classifications of cells with lightning activity. As indicated in Sect. 4.2, the specific snow water and ice water content significantly capture attention, with peak interest occurring at a geopotential height of approximately 4000 m and 7000 m (cswc), and at heights of 9000 m and 11000 m (ciwc) respectively. The neural network discovered by itself the essential ingredient for lightning, namely charge separation. It occurs when ice crystals (ciwc) and larger frozen particles (graupel, cswc) are present in the convective updraft. Once the graupel is sufficiently heavy, its velocity is smaller than the velocity of the rising ice crystals, and the collisions between ice crystals and graupel result in oppositely charged particles (Reynolds et al., 1957; Saunders et al., 2006). Fig. 1 in Lopez (2016) shows the typical distribution

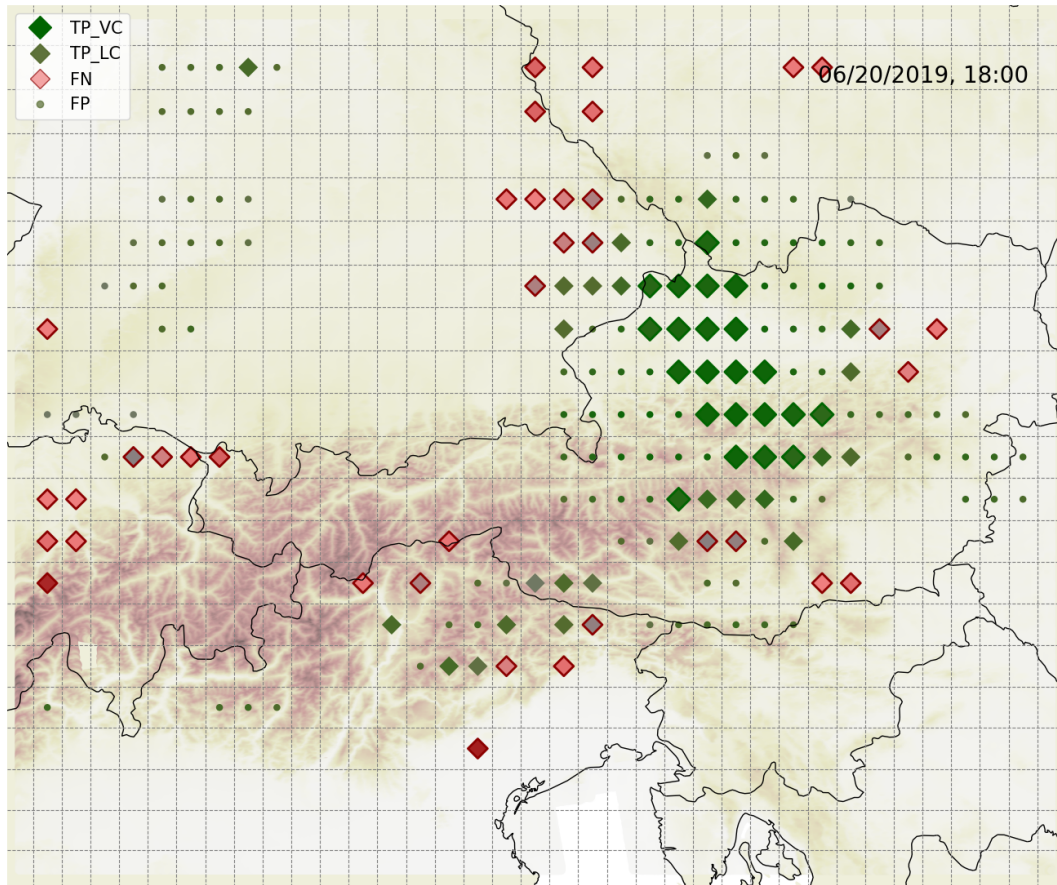


**Figure 7.** The map shows ERA5 grid cells with classifications of true positive (green diamonds), false negative (red diamonds) and false positive (dots) for the test data case June 20, 2019, in the hour before 18:00 UTC which is a case of the unseen test data. The size of the green diamonds indicates whether it is a *very* or *less* confident true positive. Low saturation of the red diamonds indicates that the output of the network was close to labeling the cell as one with lightning activity. The data for the displayed topography layer is taken from TanDEM-X (Rizzoli et al., 2017).

of charges in a mature thunderstorm cloud. However, it is noteworthy that the model seems to be particularly interested in the cloud ice water content at a height of 9000 and 11000 m while recent literature usually looks at the cloud ice water content at 440 hPa (typically about 6000 m) (Finney et al., 2014, 2018; Silva et al., 2022). Focusing on the region close to the tropopause between 9000 and 11000 m means that it is crucial to vent ice particles all the way up to the tropopause and form anvils as is typical of the thunderstorm clouds.

Moreover, the model leverages the presence of southerly winds and vertical updrafts as reliable indicators for lightning occurrence especially in the northwestern Po Plain. Additionally, high specific humidity below 4000 m serves as a robust proxy in the central and eastern Po Plain, as well as in the southern regions of the Slovenian Alps.

The results in this work suggest promising future applications. Being able to train a neural network directly on atmospheric soundings with good ability to distinguish between cells with and without lightning activity, and then opening the black box may enable researchers to gain a better understanding of atmospheric processes in regions like e.g. equatorial Africa where ample studies are scarce (Chakraborty et al., 2022). The first MGT-I satellite was launched on 13 December 2022 and will provide a lightning imager (Holmlund et al., 2021) which appears to be a promising source for the target variable. Furthermore, many existing models come with two very different parameterizations for ocean and land (Finney et al., 2014) and this inevitably leads to discontinuities in coastal areas. Also the reasons for the much lower lightning frequency over ocean are not as well understood yet. Explainable AI might be a valuable building block in moving towards a more holistic understanding of the underlying atmospheric processes.

Future work might improve the results presented in this study. Convection and cloud processes are not purely vertical processes and thus ML parameterization greatly benefits from using multiple neighboring vertical atmospheric columns instead of a single column. Wang et al. (2022) work with  $192 \text{ km} \times 192 \text{ km}$  grid cells to model, among others, subgrid zonal and meridional momentum flux due to vertical advection and suggest that a  $3 \times 3$  subgrid could further improve the performance of the deep learning approach. Here, a simple fully connected neural network is used and therefore the model loses information about the connectivity of the values along the levels of the vertical profiles. Using convolutional layers to process the profiles would, most likely, further improve the results. However, the goal of this work was to use a very simple machine learning approach to detect cells with lightning activity and then to dissect the model to understand which atmospheric conditions the model has found to be typical for lightning. The input data was preprocessed with only very little meteorological expertise to ensure that the methodology is easily transferable to other regions of the earth where the understanding of lightning related atmospheric processes is still scarce.

*Code and data availability.* The software (version 1.1; Python and R code) used to produce the results and plots in this manuscript is licenced under MIT and published on GitHub [https://github.com/noxthot/xai\\_lightningprocesses](https://github.com/noxthot/xai_lightningprocesses) (Ehrensperger et al., 2024). The source code relies on two data sources:

1. ERA5 (Hersbach et al., 2020) data are available via the Climate Data Store (Hersbach et al., 2018, 2017). Scripts for sending the retrievals are included in the `data-preprocessing` directory of the GitHub repository (Ehrensperger et al., 2024).

2. The ALDIS data (Schulz et al., 2016), which are the second important source of data, cannot be made available to the public. However, ALDIS data are available on request from ALDIS [aldis@ove.at](mailto:aldis@ove.at) – fees may be charged.

*Author contributions.* **Gregor Ehrensperger:** Methodology, Software - model & explainable AI & plotting & data preparation, Writing – original draft. **Thorsten Simon:** Data curation, Software - reference model & plotting, Writing – original draft. **Georg Mayr:** Supervision, Writing - review & editing. **Tobias Hell:** Conceptualization, Methodology.

*Competing interests.* The authors declare that they have no known competing financial interests or personal relationships that could have appeared to influence the work reported in this paper.

*Acknowledgements.* We are grateful for data support by Gerhard Diendorfer and Wolfgang Schulz from OVE-ALDIS. We thank Deborah Morgenstern and Johannes Horak for their script to compute geopotential height on ERA5 model levels. Also, we thank Johanna Rissbacher for contributing parts of Fig. 7 and the corresponding code.

*Financial support.* This work was funded by the Austrian Science Fund (FWF, grant no. P 31836) and the Austrian Research Promotion Agency (FFG, grant no. 872656).



## References

- Aas, K., Jullum, M., and Løland, A.: Explaining Individual Predictions when Features are Dependent: More Accurate Approximations to Shapley Values, *Artificial Intelligence*, 298, 103–502, <https://doi.org/10.1016/j.artint.2021.103502>, 2021.
- Allen, D. J. and Pickering, K. E.: Evaluation of Lightning Flash Rate Parameterizations for Use in a Global Chemical Transport Model, *Journal of Geophysical Research: Atmospheres*, 107, ACH 15–1–ACH 15–21, <https://doi.org/10.1029/2002JD002066>, 2002.
- Barnes, E. A., Toms, B., Hurrell, J. W., Ebert-Uphoff, I., Anderson, C., and Anderson, D.: Indicator Patterns of Forced Change Learned by an Artificial Neural Network, *Journal of Advances in Modeling Earth Systems*, 12, e2020MS002195, <https://doi.org/10.1029/2020MS002195>, 2020.
- Becerra, M., Long, M., Schulz, W., and Thottappillil, R.: On the Estimation of the Lightning Incidence to Offshore Wind Farms, *Electric Power Systems Research*, 157, 211–226, <https://doi.org/10.1016/j.epr.2017.12.008>, 2018.
- Brisson, E., Blahak, U., Lucas-Picher, P., Purr, C., and Ahrens, B.: Contrasting Lightning Projection Using the Lightning Potential Index Adapted in a Convection-Permitting Regional Climate Model, *Climate Dynamics*, 57, 2037–2051, <https://doi.org/10.1007/s00382-021-05791-z>, 2021.
- Brook, M., Nakano, M., Krehbiel, P., and Takeuti, T.: The electrical structure of the hokuriku winter thunderstorms, *Journal of Geophysical Research: Oceans*, 87, 1207–1215, <https://doi.org/10.1029/JC087iC02p01207>, 1982.
- Cecil, D. J., Buechler, D. E., and Blakeslee, R. J.: Gridded Lightning Climatology from TRMM-LIS and OTD: Dataset Description, *Atmospheric Research*, 135, 404–414, <https://doi.org/10.1016/j.atmosres.2012.06.028>, 2014.
- Chakraborty, R., Menghal, P., Harshitha, M., and Sodunke, M.: Climatology of Lightning Activities Across the Equatorial African Region, in: 2022 3rd URSI Atlantic and Asia Pacific Radio Science Meeting (AT-AP-RASC), pp. 1–4, IEEE, <https://doi.org/10.23919/AT-AP-RASC54737.2022.9814276>, 2022.
- Charn, A. B. and Parishani, H.: Predictive Proxies of Present and Future Lightning in a Superparameterized Model, *Journal of Geophysical Research: Atmospheres*, 126, <https://doi.org/10.1029/2021JD035461>, 2021.
- Cummins, K., Krider, E., and Malone, M.: The US National Lightning Detection Network and Applications of Cloud-to-Ground Lightning Data by Electric Power Utilities, *IEEE Transactions on Electromagnetic Compatibility*, 40, 465–480, <https://doi.org/10.1109/15.736207>, 1998.
- DeCaria, A. J., Pickering, K. E., Stenchikov, G. L., and Ott, L. E.: Lightning-Generated  $\text{NO}_x$  and its Impact on Tropospheric Ozone Production: A Three-Dimensional Modeling Study of a Stratosphere-Troposphere Experiment: Radiation, Aerosols and Ozone (STRAO-A) Thunderstorm, *Journal of Geophysical Research: Atmospheres*, 110, <https://doi.org/10.1029/2004JD005556>, 2005.
- Dutta, D. and Pal, S. K.: Interpretation of Black Box for Short-Term Predictions of Pre-Monsoon Cumulonimbus Cloud Events over Kolkata, *Journal of Data, Information and Management*, 4, 167–183, <https://doi.org/10.1007/s42488-022-00071-9>, 2022.
- Ehrensperger, G., Hell, T., Mayr, G., and Simon, T.: xai\_lightningprocesses, <https://doi.org/10.5281/zenodo.10899180>, 2024.
- Feldmann, M., Germann, U., Gabella, M., and Berne, A.: A Characterisation of Alpine Mesocyclone Occurrence, *Weather and Climate Dynamics*, 2, 1225–1244, <https://doi.org/10.5194/wcd-2-1225-2021>, 2021.
- Finney, D. L., Doherty, R. M., Wild, O., Huntrieser, H., Pumphrey, H. C., and Blyth, A. M.: Using Cloud Ice Flux to Parametrise Large-Scale Lightning, *Atmospheric Chemistry and Physics*, 14, 12 665–12 682, <https://doi.org/10.5194/acp-14-12665-2014>, 2014.
- Finney, D. L., Doherty, R. M., Wild, O., Stevenson, D. S., MacKenzie, I. A., and Blyth, A. M.: A Projected Decrease in Lightning under Climate Change, *Nature Climate Change*, 8, 210–213, <https://doi.org/10.1038/s41558-018-0072-6>, 2018.

- Groenemeijer, P., Púčik, T., Tsonevsky, I., and Bechtold, P.: An Overview of Convective Available Potential Energy and Convective Inhibition provided by NWP models for operational forecasting, <https://doi.org/10.21957/q392hofrl>, 2019.
- Hersbach, H., Bell, B., Berrisford, P., Hirahara, S., Horányi, A., Muñoz-Sabater, J., Nicolas, J., Peubey, C., Radu, R., Schepers, D., Simmons, A., Soci, C., Abdalla, S., Abellan, X., Balsamo, G., Bechtold, P., Biavati, G., Bidlot, J., Bonavita, M., De Chiara, G., Dahlgren, P., Dee, D., Diamantakis, M., Dragani, R., Flemming, J., Forbes, R., Fuentes, M., Geer, A., Haimberger, L., Healy, S., Hogan, R., Hólm, E., Janisková, M., Keeley, S., Laloyaux, P., Lopez, P., Lupu, C., Radnoti, G., de Rosnay, P., Rozum, I., Vamborg, F., Villaume, S., and Thépaut, J.-N.: Complete ERA5 from 1979: Fifth generation of ECMWF atmospheric reanalyses of the global climate, <https://cds.climate.copernicus.eu#!/home>, accessed on 27-05-2021, 2017.
- Hersbach, H., Bell, B., Berrisford, P., Biavati, G., Horányi, A., Muñoz Sabater, J., Nicolas, J., Peubey, C., Radu, R., Rozum, I., Schepers, D., Simmons, A., Soci, C., Dee, D., and Thépaut, J.-N.: ERA5 hourly data on single levels from 1959 to present, <https://doi.org/10.24381/cds.adbb2d47>, accessed on 16-02-2022, 2018.
- Hersbach, H., Bell, B., Berrisford, P., Hirahara, S., Horányi, A., Muñoz-Sabater, J., Nicolas, J., Peubey, C., Radu, R., Schepers, D., Simmons, A., Soci, C., Abdalla, S., Abellan, X., Balsamo, G., Bechtold, P., Biavati, G., Bidlot, J., Bonavita, M., De Chiara, G., Dahlgren, P., Dee, D., Diamantakis, M., Dragani, R., Flemming, J., Forbes, R., Fuentes, M., Geer, A., Haimberger, L., Healy, S., Hogan, R. J., Hólm, E., Janisková, M., Keeley, S., Laloyaux, P., Lopez, P., Lupu, C., Radnoti, G., de Rosnay, P., Rozum, I., Vamborg, F., Villaume, S., and Thépaut, J.-N.: The ERA5 Global Reanalysis, *Quarterly Journal of the Royal Meteorological Society*, 146, 1999–2049, <https://doi.org/10.1002/qj.3803>, 2020.
- Hilburn, K. A., Ebert-Uphoff, I., and Miller, S. D.: Development and Interpretation of a Neural-Network-Based Synthetic Radar Reflectivity Estimator Using GOES-R Satellite Observations, *Journal of Applied Meteorology and Climatology*, 60, 3–21, <https://doi.org/10.1175/JAMC-D-20-0084.1>, 2021.
- Holle, R. L.: A Summary of Recent National-Scale Lightning Fatality Studies, *Weather, Climate, and Society*, 8, 35–42, <https://doi.org/10.1175/WCAS-D-15-0032.1>, 2016.
- Holmlund, K., Grandell, J., Schmetz, J., Stuhlmann, R., Bojkov, B., Munro, R., Lekouara, M., Coppens, D., Viticchie, B., August, T., Theodore, B., Watts, P., Dobber, M., Fowler, G., Bojinski, S., Schmid, A., Salonen, K., Tjemkes, S., Aminou, D., and Blythe, P.: Meteosat Third Generation (MTG): Continuation and Innovation of Observations from Geostationary Orbit, *Bulletin of the American Meteorological Society*, 102, 990–1015, <https://doi.org/10.1175/BAMS-D-19-0304.1>, 2021.
- Houze, R. A.: Orographic Effects on Precipitating Clouds, *Reviews of Geophysics*, 50, 1–47, <https://doi.org/10.1029/2011RG000365>, 2012.
- Lopez, P.: A Lightning Parameterization for the ECMWF Integrated Forecasting System, *Monthly Weather Review*, 144, 3057–3075, <https://doi.org/10.1175/MWR-D-16-0026.1>, 2016.
- Lou, Y., Caruana, R., and Gehrke, J.: Intelligible Models for Classification and Regression, in: *Proceedings of the 18th ACM SIGKDD International Conference on Knowledge Discovery and Data Mining, KDD '12*, pp. 150–158, Association for Computing Machinery, New York, NY, USA, ISBN 9781450314626, <https://doi.org/10.1145/2339530.2339556>, 2012.
- Lundberg, S. M. and Lee, S.-I.: A Unified Approach to Interpreting Model Predictions, in: *Advances in Neural Information Processing Systems*, edited by Guyon, I., Luxburg, U. V., Bengio, S., Wallach, H., Fergus, R., Vishwanathan, S., and Garnett, R., vol. 30, Curran Associates, Inc., <https://proceedings.neurips.cc/paper/2017/file/8a20a8621978632d76c43dfd28b67767-Paper.pdf>, 2017.
- Mayer, K. J. and Barnes, E. A.: Subseasonal Forecasts of Opportunity Identified by an Explainable Neural Network, *Geophysical Research Letters*, 48, e2020GL092092, <https://doi.org/10.1029/2020GL092092>, 2021.

- McCaul, E. W., Goodman, S. J., LaCasse, K. M., and Cecil, D. J.: Forecasting Lightning Threat Using Cloud-Resolving Model Simulations, *Weather and Forecasting*, 24, 709–729, <https://doi.org/10.1175/2008WAF2222152.1>, 2009.
- Morgenstern, D., Stucke, I., Simon, T., Mayr, G. J., and Zeileis, A.: Differentiating Lightning in Winter and Summer with Characteristics of the Wind Field and Mass Field, *Weather and Climate Dynamics*, 3, 361–375, <https://doi.org/10.5194/wcd-3-361-2022>, 2022.
- Morgenstern, D., Stucke, I., Mayr, G. J., Zeileis, A., and Simon, T.: Thunderstorm environments in Europe, *Weather and Climate Dynamics*, 4, 489–509, <https://doi.org/10.5194/wcd-4-489-2023>, 2023.
- Murray, L. T.: An Uncertain Future for Lightning, *Nature Climate Change*, 8, 191–192, <https://doi.org/10.1038/s41558-018-0094-0>, 2018.
- Price, C. and Rind, D.: A Simple Lightning Parameterization for Calculating Global Lightning Distributions, *Journal of Geophysical Research: Atmospheres*, 97, 9919–9933, <https://doi.org/10.1029/92JD00719>, 1992.
- Reineking, B., Weibel, P., Conedera, M., and Bugmann, H.: Environmental Determinants of Lightning- v. Human-Induced Forest Fire Ignitions Differ in a Temperate Mountain Region of Switzerland, *International Journal of Wildland Fire*, 19, 541–557, <https://doi.org/10.1071/WF08206>, 2010.
- Reynolds, S., Brook, M., and Gourley, M. F.: Thunderstorm Charge Separation, *Journal of Atmospheric Sciences*, 14, 426–436, [https://doi.org/10.1175/1520-0469\(1957\)014<0426:TCS>2.0.CO;2](https://doi.org/10.1175/1520-0469(1957)014<0426:TCS>2.0.CO;2), 1957.
- Ritenour, A. E., Morton, M. J., McManus, J. G., Barillo, D. J., and Cancio, L. C.: Lightning Injury: A Review, *Burns*, 34, 585–594, <https://doi.org/10.1016/j.burns.2007.11.006>, 2008.
- Rizzoli, P., Martone, M., Gonzalez, C., Wecklich, C., Borla Tridon, D., Bräutigam, B., Bachmann, M., Schulze, D., Fritz, T., Huber, M., Wesel, B., Krieger, G., Zink, M., and Moreira, A.: Generation and performance assessment of the global TanDEM-X digital elevation model, *ISPRS Journal of Photogrammetry and Remote Sensing*, 132, 119–139, <https://doi.org/https://doi.org/10.1016/j.isprsjprs.2017.08.008>, 2017.
- Romps, D. M., Charn, A. B., Holzworth, R. H., Lawrence, W. E., Molinari, J., and Vollaro, D.: CAPE Times P Explains Lightning Over Land But Not the Land-Ocean Contrast, *Geophysical Research Letters*, 45, 12,623–12,630, <https://doi.org/10.1029/2018GL080267>, 2018.
- Saunders, C. P. R., Bax-norman, H., Emersic, C., Avila, E. E., and Castellano, N. E.: Laboratory Studies of the Effect of Cloud Conditions on Graupel/Crystal Charge Transfer in Thunderstorm Electrification, *Quarterly Journal of the Royal Meteorological Society*, 132, 2653–2673, <https://doi.org/10.1256/qj.05.218>, 2006.
- Schulz, W., Diendorfer, G., Pedebay, S., and Poelman, D. R.: The European Lightning Location System EUCLID Part 1: Performance Analysis and Validation, *Natural Hazards and Earth System Sciences*, 16, 595–605, <https://doi.org/10.5194/nhess-16-595-2016>, 2016.
- Shan, S., Allen, D., Li, Z., Pickering, K., and Lapierre, J.: Machine-learning-based investigation of the variables affecting summertime lightning occurrence over the Southern Great Plains, 23, 14 547–14 560, <https://doi.org/10.5194/acp-23-14547-2023>, 2023.
- Shapley, L. S.: A Value for N-Person Games, RAND Corporation, Santa Monica, CA, <https://doi.org/10.7249/P0295>, 1952.
- Shi, M., Zhang, W., Fan, P., Chen, Q., Liu, Z., Li, Q., and Liu, X.: Modelling Deep Convective Activity Using Lightning Clusters and Machine Learning, *International Journal of Climatology*, 42, 952–973, <https://doi.org/10.1002/joc.7282>, 2022.
- Silva, S. J., Keller, C. A., and Hardin, J.: Using an Explainable Machine Learning Approach to Characterize Earth System Model Errors: Application of SHAP Analysis to Modeling Lightning Flash Occurrence, *Journal of Advances in Modeling Earth Systems*, 14, e2021MS002 881, <https://doi.org/10.1029/2021MS002881>, 2022.
- Simon, T., Mayr, G., Morgenstern, D., Umlauf, N., and Zeileis, A.: Amplification of annual and diurnal cycles of alpine lightning, *Climate Dynamics*, 61, 1–13, <https://doi.org/10.1007/s00382-023-06786-8>, 2023.

- Srivastava, N., Hinton, G., Krizhevsky, A., Sutskever, I., and Salakhutdinov, R.: Dropout: A Simple Way to Prevent Neural Networks from Overfitting, *Journal of Machine Learning Research*, 15, 1929–1958, <http://jmlr.org/papers/v15/srivastava14a.html>, 2014.
- Stirnberg, R., Cermak, J., Kotthaus, S., Haeffelin, M., Andersen, H., Fuchs, J., Kim, M., Petit, J.-E., and Favez, O.: Meteorology-Driven Variability of Air Pollution (PM<sub>1</sub>) Revealed with Explainable Machine Learning, *Atmospheric Chemistry and Physics*, 21, 3919–3948, <https://doi.org/10.5194/acp-21-3919-2021>, 2021.
- Takahashi, T., Sugimoto, S., Kawano, T., and Suzuki, K.: Microphysical Structure and Lightning Initiation in Hokuriku Winter Clouds, 124, 13 156–13 181, <https://doi.org/10.1029/2018JD030227>, 2019.
- Takeuti, T., Nakano, M., Brook, M., Raymond, D. J., and Krehbiel, P.: The anomalous winter thunderstorms of the Hokuriku Coast, 83, 2385–2394, <https://doi.org/10.1029/JC083iC05p02385>, 1978.
- Tippett, M. K., Lepore, C., Koshak, W. J., Chronis, T., and Vant-Hull, B.: Performance of a Simple Reanalysis Proxy for U.S. Cloud-to-Ground Lightning, *International Journal of Climatology*, 39, 3932–3946, <https://doi.org/10.1002/joc.6049>, 2019.
- Toms, B. A., Barnes, E. A., and Hurrell, J. W.: Assessing Decadal Predictability in an Earth-System Model Using Explainable Neural Networks, *Geophysical Research Letters*, 48, e2021GL093 842, <https://doi.org/10.1029/2021GL093842>, 2021.
- Tost, H., Jöckel, P., and Lelieveld, J.: Lightning and Convection Parameterisations – Uncertainties in Global Modelling, *Atmospheric Chemistry and Physics*, 7, 4553–4568, <https://doi.org/10.5194/acp-7-4553-2007>, 2007.
- Ukkonen, P. and Mäkelä, A.: Evaluation of Machine Learning Classifiers for Predicting Deep Convection, *J. Adv. Model. Earth Sy.*, 11, 1784–1802, <https://doi.org/10.1029/2018MS001561>, 2019.
- Ukkonen, P., Manzato, A., and Mäkelä, A.: Evaluation of Thunderstorm Predictors for Finland Using Reanalyses and Neural Networks, *Journal of Applied Meteorology and Climatology*, 56, 2335–2352, <https://doi.org/10.1175/JAMC-D-16-0361.1>, 2017.
- van der Velden, B. H., Kuijff, H. J., Gilhuijs, K. G., and Viergever, M. A.: Explainable artificial intelligence (XAI) in deep learning-based medical image analysis, *Medical Image Analysis*, 79, 102 470, <https://doi.org/10.1016/j.media.2022.102470>, 2022.
- Wang, D., Zheng, D., Wu, T., and Takagi, N.: Winter Positive Cloud-to-Ground Lightning Flashes Observed by LMA in Japan, 16, 402–411, <https://doi.org/10.1002/tee.23310>, 2021.
- Wang, P., Yuval, J., and O’Gorman, P. A.: Non-local parameterization of atmospheric subgrid processes with neural networks, *Journal of Advances in Modeling Earth Systems*, p. e2022MS002984, <https://doi.org/10.1029/2022MS002984>, 2022.
- Wood, S. N.: *Generalized Additive Models: An Introduction with R*, Texts in Statistical Science, Chapman & Hall/CRC, Boca Raton, 2nd edn., <https://doi.org/10.1201/9781420010404>, 2017.
- Wood, S. N., Li, Z., Shaddick, G., and Augustin, N. H.: Generalized Additive Models for Gigadata: Modeling the U.K. Black Smoke Network Daily Data, *Journal of the American Statistical Association*, 112, 1199–1210, <https://doi.org/10.1080/01621459.2016.1195744>, 2017.
- Zhang, Y., Tiño, P., Leonardis, A., and Tang, K.: A Survey on Neural Network Interpretability, *IEEE Transactions on Emerging Topics in Computational Intelligence*, 5, 726–742, <https://doi.org/10.1109/TETCI.2021.3100641>, 2021.